ARTICLE

# Excited State Deactivation via Solvent to Chromophore Proton Transfer in Isolated 1:1 Molecular Complex: Experimental Validation by Measuring the Energy Barrier and Kinetic Isotope Effect

Saurabh Khodia,[‡,a] Ramesh Jarupula,[‡,a] Simran Baweja,[a] Md. Shabeeb,[a] Bhavika Kalal[a] and Surajit Maity*[,a]

**ABSTRACT:** We have experimentally demonstrated conclusive evidence of solvent-to-chromophore excited state proton transfer (ESPT) as a deactivation mechanism in a binary complex isolated in the gas phase. The above was achieved by determining the energy barrier of the ESPT processes, qualitatively analysing the quantum tunnelling rates and evaluating the kinetic isotope effect. The 1:1 complexes of 2,2'-pyridylbenzimidazole (PBI) with $H_2O$, $D_2O$ and $NH_3$, produced in a supersonic jet-cooled molecular beam, were characterised spectroscopically. The vibrational frequencies of the complexes in the $S_1$ electronic state were recorded using a resonant two-colour two-photon ionization method coupled to a Time-of-Flight mass spectrometer set-up. In the PBI-$H_2O$, the ESPT energy barrier of 431±10 $cm^{-1}$ was measured using UV-UV hole-burning spectroscopy. The exact reaction pathway was experimentally determined by isotopic substitution of the tunnelling-proton (in PBI-$D_2O$) and increasing the width of the proton transfer barrier (in PBI-$NH_3$). In both cases, the energy barrier was significantly increased to > 1030 $cm^{-1}$ in the PBI-$D_2O$ and to > 868 $cm^{-1}$ in PBI-$NH_3$. The heavy atom in PBI-$D_2O$ decreased the zero-point energy in the $S_1$ state significantly, resulting in the elevation of the energy barrier. Secondly, the solvent-to-chromophore proton tunnelling was found to decrease drastically upon deuterium substitution. In the PBI-$NH_3$ complex, the solvent molecule formed a preferential hydrogen bonding with the acidic (PBI)N-H group. This led to the formation of a weak hydrogen bonding between the ammonia and the pyridyl-N atom, thus, increasing the proton transfer barrier width ($H_2N$-H$\cdots N_{pyridyl}$(PBI)). The above resulted in increased barrier height and decreased quantum tunnelling rate in the excited state. The experimental investigation, aided by computational investigations, demonstrated conclusive evidence of a novel deactivation channel of an electronically excited biologically relevant system. The variation observed for the energy barrier and the quantum tunnelling rate by substituting $NH_3$ in place of $H_2O$ can be directly correlated to the drastically different photo-chemical and photo-physical reactions of biomolecules under various microenvironments.

## Introduction

Excited state proton and hydrogen atom transfer processes are considered vital reactions in the biomolecules upon absorption of UV radiation.[1,2] The investigations based on femtosecond chemistry revealed that most of the biomolecules undergo efficient excited-state deactivation through rapid decay pathways.[3–6] The state-of-art experiments and theoretical studies have shown that the deactivation process is mainly driven by the nonadiabatic dynamics on the complex potential energy surface.[7,8] In nucleic bases, the electronic energy of the excited state is found to be dissipated via internal conversion associated with ultrafast ring puckering motions at a picosecond time scale.[1] Interestingly, isolated organic molecules like azaindole derivatives,[9] phenol,[10] naphthol[11] and 2-aminopyridine,[12] 7-hydroxyquinoline[13] systems having rigid conjugated rings without an apparent twisting coordinate could also maintain their integrity under intense UV light owing to the available proton transfer channel leading to nonadiabatic decay.

Investigation of excited state proton (ESPT) and hydrogen (ESHT) transfer processes in gas phase molecular complexes using laser spectroscopic investigations have been studied over the last two decades. Such investigations provide a perfect platform for both energy-resolved and time-resolved investigations of real-time even very accurately.[10] The photo-acidity of the -NH, -OH groups present in the above bio-relevant molecules drastically increased upon UV excitation.[14] This allows the relay of hydrogen[10] and proton[13] to the solvent molecules to either tautomerisation and/or deactivation under appropriate circumstances. Similarly, the photo-basicity of the hydrogen-bonding partner has also been found to be the key deciding factor in initiating the excited state proton transfer process because of its direct involvement with the reaction.[15] The most discussed studies on ESPT and ESHT processes have been the ammonia complexes of naphthol and phenol.[10] Most importantly, the gas phase studies reveal that the proton

transfer is directional and initiated by the transfer of a proton from the chromophore to the solvent molecule, which is followed by the deactivation via internal conversion (other than the tautomerisation process) [9–13]

Recently, the proton transfer mechanism revealed in the isolated PBI–$H_2O$ clusters has shown that the proton transfer is from solvent to the PBI molecule,[16] unlike the commonly observed process from chromophore to solvent.[11,13,17] The above investigations revealed that the ESPT processes were only triggered in systems with a minimum of three solvent molecules. However, a hydrogen atom transfer reaction was known to be observed in the phenol-$NH_3$ cluster as well.[10] The experimental reports of proton transfer involving a single solvent molecule as a proton donor have not been reported in the literature, except PBI-$H_2O$ complex.[16]

The PBI complex with different solvents will be a good candidate to explore the mechanism and controlling factors governing the excited state proton transfer process. In addition, these systems can serve as a mimetic model for base-pairing with O-H···N type of hydrogen bonding to explore the deactivation channels associated with proton transfer. The PBI molecule incorporates a benzimidazole ring connected to a pyridine ring via a single C-C bond. The molecule is widely used as a ligand in organometallic complexes to provide functionality owing to its widespread bioactivity because of the presence of the benzimidazole moiety.[18–24] Additionally, the pyridine-N receiving hydrogen or proton can lead to the formation of a tautomeric structure, which has been considered the key intermediate in photo-catalytic water splitting using the N-containing bases. [25]

In the present article, we have considered binary complexes of 2,2'-pyridylbenzimidazole (PBI) with $H_2O/D_2O$ and $NH_3$ to convincingly prove the solvent to chromophore proton transfer processes, which leads to the deactivation of the excited complex. The above study certainly gives a new dimension to the deactivation mechanism of photo-excited N-containing biomolecules.

## Method

**Experimental:** In a differentially pumped molecular beam machine, the binary complexes of PBI–$H_2O$, PBI-$D_2O$ and PBI-$NH_3$ were produced under the supersonic condition. The detail of the molecular beam set-up is described elsewhere.[16,26,27] The PBI (Sigma-Aldrich, 97%) was heated to 393K to obtain sufficient vapour pressure, which was co-expanded with the vapours of $H_2O/D_2O/NH_3$ seeded in 2 bar of He in the vacuum. The complexes were characterised using resonant two-colour two-photon ionization (R2PI) and hole-burning (HB) spectroscopies. In R2PI spectroscopy, the jet-cooled molecular complexes were electronically excited using a frequency-doubled output of a tunable dye laser pumped by the second harmonic of an Nd:YAG laser (pulsed width 5 ns and resolution ~0.3 $cm^{-1}$). The ionization laser was the 4$^{th}$ harmonic of the same Nd:YAG laser to avoid pulse-to-pulse temporal jitter. The produced ions were recorded by monitoring the m/z ratio of 195 (PBI), 213 (PBI–$H_2O$), 215 (PBI–$D_2O$) and 212 (PBI-$NH_3$) amu in a 1-meter linear time-of-flight (TOF) mass spectrometer equipped with an MCP detector. For the hole-burning spectroscopy, a third hole-burning laser (second harmonic output of a dye laser pumped by a second Nd:YAG laser) is introduced 200 ns prior to the excitation and ionization lasers. The hole-burning laser is scanned while the excitation laser is fixed at the $S_0 \rightarrow S_1$ electronic origin of the PBI–$H_2O$ complex. A dip is observed in the R2PI signal at each resonant hole-burning laser wavenumber, as the above process depopulated the ground state irrespective of the lifetime of the final excited vibrational state. As the excitation laser signal was directly dependent on the ground state population, a negative-going peak was observed for each resonant HB laser. The HB spectrum thus can measure the excited state vibrational frequencies regardless of the lifetime of the higher vibrational levels in the $S_1$ state. All the experiments were carried out with ~0.2 mJ per pulse of UV laser power with a beam size of ~2 mm.

**Computational:** All the calculations were performed with the TURBOMOLE program using the resolution-of-the-identity (RI) approximation.[28] The ground and excited state geometry optimisations and the potential-energy profiles were calculated using the dispersion corrected density functional theory (DFT-D4) method with B3LYP density functional and the polarization functional def2-TZVPP/def2-TZVP basis set.[29–32] All the Time-Dependent Density Functional Theory (TDDFT) calculations were done using Tamm–Dancoff approximation (TDA). The initial structures of the PBI–S complexes were generated by placing the solvent molecules around the PBI molecule in such a way that it formed a molecular bridge between the pyridine N and the benzimidazole NH groups. The optimised structures were further verified using subsequent frequency calculations at the same level of theory.

A detailed description of the calculation of ESPT and ESHT processes is given elsewhere.[16,33] In brief, the initial geometry of the proton transfer (PT) state of the PBI–S complex was generated by adding a hydroxide ion $OH^-$ (for PBI-$H_2O$ complex) and $NH2^-$ (for PBI-$NH_3$ complex) to the protonated PBI cation ($PBIH^+$) forming hydrogen-bond between the NH groups. Subsequently, the potential energy profiles (PES) were calculated for the ESPT and ESHT pathways by scanning the $N_P$···H bond length along the proton-transfer and hydrogen transfer, respectively. The optimised ground-state and the excited-state geometry of the PBI-$H_2O$ and PBI-$NH_3$ complex (Cartesian coordinates given in SI Table S2) were used to calculate the Franck–Condon simulations. The Franck–Condon simulations were performed using the FC-LabWin program developed by Pugliesi et al.[34] The resolution of the simulated spectrum was set at 0.5 $cm^{-1}$ to compare with the observed spectral bandwidth.

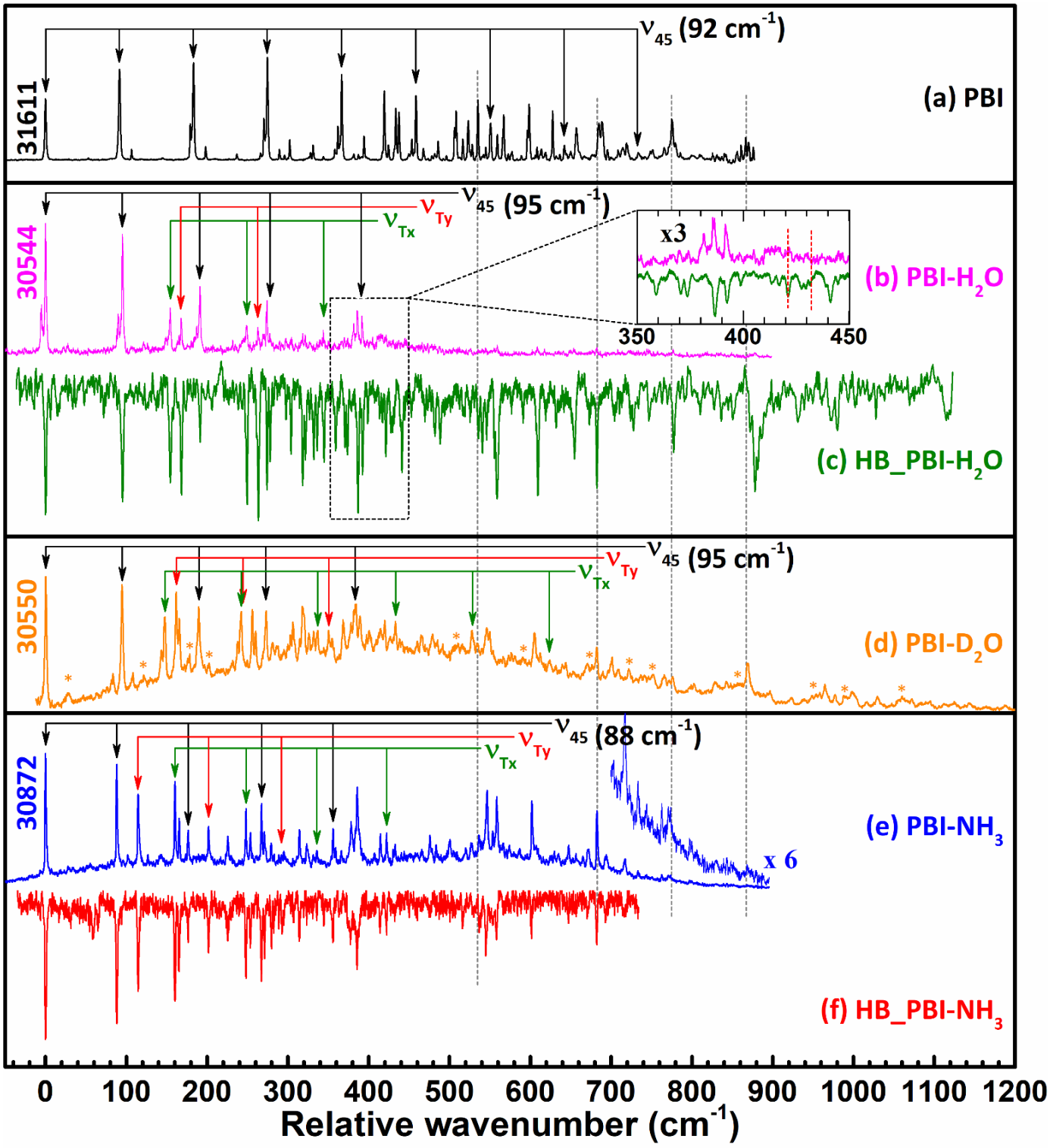


**Figure 1.** The two-color resonant two-photon ionization (R2PI) spectra of the $S_0 \rightarrow S_1$ band system of PBI (trace a), PBI-$H_2O$ (trace b), PBI-$D_2O$ (trace d) and PBI-$NH_3$ (trace e). The connected vertical arrows in trace a show the progression of $\nu_{45}$ modes. The hole-burning spectra of PBI-$H_2O$ (trace c) and PBI-$NH_3$ (trace f) complexes were recorded by fixing the probe laser at the respective origin bands while scanning the hole-burning laser 200 ns prior to the other. The vertical dashed lines represent the last observed bands (intramolecular) in R2PI spectra.

## Result and discussion

**Electronic spectra of PBI-S complexes:** Figure 1 shows the two-colour resonant two-photon ionization (R2PI) spectra of PBI (trace a), PBI-$H_2O$ (trace b), PBI-$D_2O$ (trace d), and PBI-$NH_3$ (trace e) recorded by monitoring the ion signal at the m/z of 195, 213, 215 and 212 amu. The band origins of the $S_0 \rightarrow S_1$ transitions of PBI, PBI-$H_2O$, PBI-$D_2O$, and PBI-$NH_3$ are positioned at 30611, 30544, 30550, and 30872 $cm^{-1}$, respectively. Upon complexation, the band origins of $H_2O$, $D_2O$ and $NH_3$ complexes of PBI have shown large shifts ($\Delta\nu$) of −1067, −1061 and −739 $cm^{-1}$, respectively. The above suggests the greater stabilisation of the electronically excited molecular complexes. The inverted traces shown in Figures 1c and 1f are the UV-UV hole-burning (HB) spectra of the PBI-$H_2O$ and PBI-$NH_3$ complexes, respectively. The above two HB spectra confirm the presence of a single isomer in the observed band systems in each system.

The positions of the $S_0 \rightarrow S_1$ band origin of the PBI-S complexes are highly sensitive to the docking preferences of the ad-molecules.[1–4] A non-covalently bound Ar atom on the aromatic face of PBI resulted in a marginal (− 40 $cm^{-1}$) redshift of the origin band. On the contrary, an ad-molecule forming hydrogen bonds to the imidazolyl-NH ($N_IH$) group showed a large redshift, such as −1067 $cm^{-1}$ for PBI-$H_2O$ and −1203 $cm^{-1}$ for PBI-$CH_3OH$.[1,4] Therefore, the docking of $NH_3$ on PBI takes place via hydrogen bonding with the $N_IH$ group. The structures of the PBI-$H_2O$ and PBI-$CH_3OH$ were confirmed using IR spectroscopic characterisation of the gas phase complexes.[4]

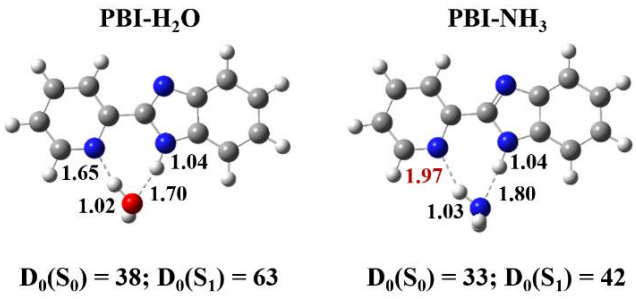


**Figure 2.** Calculated structures of PBI-$H_2O$ and PBI-$NH_3$ complexes. The calculated binding energy ($D_0$) with zero-point vibrational energy correction in the ground ($S_0$) and first electronic excited states ($S_1$) are given in kJ $mol^{-1}$.

**Structures of PBI-S Complexes:** The geometry optimised most stable structure of PBI-$H_2O$ and PBI-$NH_3$ complexes, calculated at DFT-D4/B3LYP (def2-TZVPP) level of theory, are shown in Figure 2. The calculated binding energies and a few important frequency data are given in Table 1. The structure of PBI-$H_2O$ shows $N_IH\cdots O$ and $OH\cdots N_P$ ($N_P$ = pyridinyl N) hydrogen bonds, in which the hydrogen bond length of $N_IH\cdots O$ is 1.70 Å is marginally longer than that of $OH\cdots N_P$ (1.65 Å). The experimentally measured frequency of intermolecular $\nu_{Tx}$ mode,[1] i.e., the internal translational motion of $H_2O$ along the $N_IH\cdots O$ hydrogen bond, as shown in Figure 3, is positioned at 154 $cm^{-1}$. The $\nu_{Ty}$ mode, i.e., the internal translational motion of $H_2O$ along the $OH\cdots N_P$ hydrogen bond, is observed at 168 $cm^{-1}$, which is 14 $cm^{-1}$ higher than the $\nu_{Tx}$ mode. The experimental values of $\nu_{Tx}$ and $\nu_{Ty}$ modes are in good agreement with the calculated data, as shown in Table 1. Therefore, the $OH\cdots N_P$ hydrogen bond can be considered marginally stronger than the $N_IH\cdots O$ bond. Therefore, the shorter $H\cdots N_p$ bond length can be linked with strong hydrogen bonding. In the case of PBI-$D_2O$, both $\nu_{Tx}$ and $\nu_{Ty}$ modes decrease to 148 and 162 $cm^{-1}$, respectively, due to the higher molecular weight of the solvent molecule. The bond strength order remained unchanged upon isotopic substitution.

The R2PI spectrum of PBI-$NH_3$ (Figure 1e) shows a large $\Delta\nu$ (−739 $cm^{-1}$) value, which implies docking of ammonia at the $N_IH$-site of PBI. The calculated most stable structure is shown in Figure 2, which shows $N_IH\cdots N$ and $NH\cdots N_P$ hydrogen bonding. In this, the $N_IH\cdots N$ hydrogen bond length (1.80 Å) is found to be significantly shorter than that (1.93 Å) of the $NH\cdots N_P$ bond. It suggests the presence of a weaker $NH\cdots N_P$ bond in the cluster. In this, the intermolecular $\nu_{Ty}$ mode (internal translation of $NH_3$ mode along the $NH\cdots N_P$ bond) was found to be significantly lower at 115 $cm^{-1}$ than the $\nu_{Tx}$ mode at 160 $cm^{-1}$. Note that the $\nu_{Ty}$ mode is lowered by 53 $cm^{-1}$ as compared to that in PBI-$H_2O$, implying a feebly bound $NH\cdots N_P$ hydrogen bond in the structure. The above experimental observation was in line with the calculated longer $NH\cdots N_P$ hydrogen bond length. As per the literature, $NH_3$ has higher gas phase basicity compared to water.[5] Therefore, ammonia acts as a stronger hydrogen bond acceptor than the donor. The formation of a stronger $N_IH\cdots N$ over $NH\cdots N_P$ is thus justified. Note that the $\nu_{45}$ mode (Figure 3) is the in-plane bending motion of imidazolyl and pyridyl rings with respect to the bridging C-C bond. Because of the weakly bridged $NH_3$ in the complex, the vibrational frequency of the $\nu_{45}$ mode is expected to be less than that in the PBI-$H_2O$ complex. The experimental value of $\nu_{45}$ mode in PBI-$NH_3$ (88 $cm^{-1}$) is found to be less than that in PBI-$H_2O$ (95 $cm^{-1}$), confirming the structure of the former. In addition, the binding energy values of PBI-$H_2O$ and PBI-$NH_3$ complexes in the respective $S_1$ states are 63 kJ $mol^{-1}$ and 42 kJ $mol^{-1}$ (Figure 2), suggesting lower stabilisation of the PBI-$NH_3$ complex. The above can be directly linked with the lower $|\Delta\nu|$ values of the complex compared to the water complex.

**Excited State Processes in PBI-$H_2O$:** By comparing the R2PI spectra of PBI and PBI-$H_2O$ (and PBI-$D_2O$) complex, the intramolecular modes of PBI can be easily isolated from the intermolecular modes (and its combinations with intermolecular modes). As per the assignments given in SI Figure S1, the bands in the PBI-$H_2O$ system present within $0_0^0 + 500\,cm^{-1}$ were assigned as low energy the intramolecular modes ($\nu_{45}$, $\nu_{44}$, $\nu_{43}$ and combinations of the bands) and intermolecular modes (the combination of $\nu_{Tx}/\nu_{Ty}$ with the intramolecular modes $\nu_{45}$). Similarly, the peaks associated with the intermolecular vibrations have shown decreased intensities at the higher energy region. The lowering of the intensity of higher energy bands and disappearance of peaks above 421 $cm^{-1}$ in the PBI-$H_2O$ spectrum can be explained using the following three possible photophysical and photochemical processes.

**(a) Franck-Condon Factor:** The intensity of the electronic transitions from the vibrationless $S_0$ state to the vibrationally excited $S_1$ state is dependent on the Frank-Condon factor of the transition. If the electronic structure of the complex upon electronic excitation is substantially different than that of the ground state, the Franck-Condon (FC) intensity can be very low for an electronic transition. The R2PI spectrum may disappear due to low FC factors above a certain region.

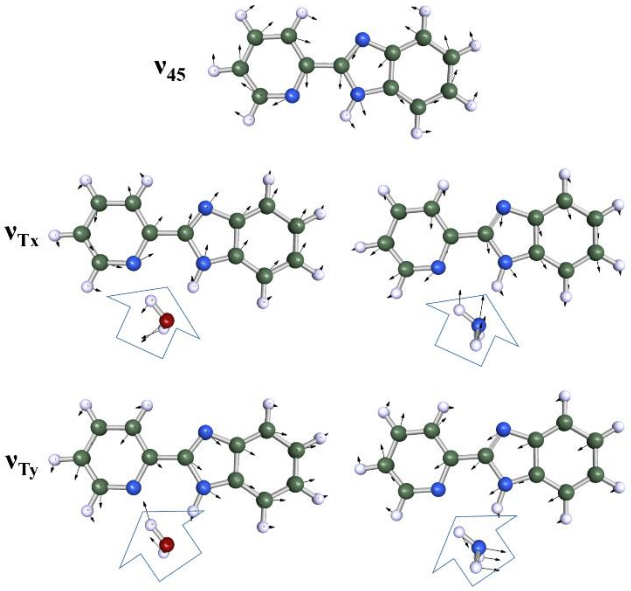


**Figure 3.** The intramolecular vibrational modes $\nu_{45}$ in PBI and $\nu_{Tx}$ and $\nu_{Ty}$ in PBI-$H_2O$ and PBI-$NH_3$ complexes are shown.

**Table 1.** The experimental band origin transitions ($0_0^0$) and spectral shifts ($\Delta\nu$) in $cm^{-1}$, and experimentally observed low energy vibrational bands ($cm^{-1}$) along with the assignments are given for PBI, PBI-$H_2O$, PBI-$D_2O$ and PBI-$NH_3$ complexes. Hydrogen bond lengths of $N_iH\cdots$(N/O) and $N_iH\cdots$(N/O) are given in Å unit. The values in parentheses are calculated scaled frequencies (scaling factor=0.85).

| | PBI | PBI-$H_2O$ | PBI-$D_2O$ | PBI-$NH_3$ |
|---|---|---|---|---|
| $0_0^0$ ($cm^{-1}$) | 31611 | 30544 | 30550 | 30872 |
| $\Delta\nu$ ($cm^{-1}$) | 0 | −1067 | −1061 | −739 |
| mode | $\nu'_{expt}$ | $\nu'_{expt}$ | $\nu'_{expt}$ | $\nu'_{expt}$ |
| $45_0^1$ | 92 | 95(95) | 95 | 88(88) |
| $Tx_0^1$ | - | 154(154) | 148 | 160(153) |
| $Ty_0^1$ | - | 168(171) | 162 | 115(124) |
| $N_iH\cdots$(N/O) | - | 1.70 | 1.68 | 1.80 |
| (O/N)H$\cdots N_P$ | - | 1.65 | 1.64 | 1.97 |

**(b) Quantum Tunnelling:** In the R2C2PI experiments, the pulse widths of the excitation and ionization lasers were 5 ns, and the laser pulses were temporally overlapped within ±1 ns. The intensity of the R2PI signal depends on the lifetime of the excited vibrational states.[6] The lifetime of the vibrationless $S_1$ state of PBI-$H_2O$ was measured to be in the same order of magnitude (~5 ns) as the laser pulses. A short lifetime in the excited $S_1$ vibrational state (<100 ps) due to enhanced quantum mechanical tunnelling of a hydrogen atom/proton can decrease and/or vanish of R2PI signals.[8,12,35]

**(c) Energy Barrier:** In addition to the above two factors, the disappearance of the R2PI peaks above $0_0^0 + 421$ $cm^{-1}$ can be due to the fast deactivation of the excited state via proton/hydrogen atom transfer reaction. The above proceeds efficiently if the molecule is excited to a state higher in energy than the energy barrier of the subsequent reaction process.[13,36]

**Table 2.** The R2PI peak positions and vibrational frequencies in $S_1$ of PBI-$H_2O$ and PBI-$D_2O$ are given in $cm^{-1}$ along with the assignment. The intensity ratios $\frac{I_D}{I_H} = \frac{I_{PBI-D_2O}}{I_{PBI-H_2O}}$ of the bands are given. Values in bold represent intramolecular bands.

| PBI-$H_2O$ | | PBI-$D_2O$ | | Assignment | $I_D/I_H$ |
|---|---|---|---|---|---|
| Positions | Freq | Positions | Freq | | |
| 30544 | 0 | 30550 | 0 | $0_0^0$ | 1.00 |
| **30639** | **95** | **30644** | **94** | $\mathbf{45_0^1}$ | **0.92** |
| 30698 | 154 | 30698 | 148 | $T_{x_0}^1$ | 1.81 |
| 30712 | 168 | 30711 | 161 | $T_{y_0}^1$ | 4.05 |
| **30735** | **191** | **30739** | **189** | $\mathbf{45_0^2}$ | **1.12** |
| 30793 | 249 | 30792 | 242 | $45_0^1T_{x_0}^1$ | 2.86 |
| 30807 | 263 | 30806 | 256 | $45_0^1T_{y_0}^1$ | 3.91 |
| **30818** | **274** | **30822** | **272** | $\mathbf{45_0^3}$ | **1.40** |
| 30848 | 303 | 30856 | 306 | $T_{x_0}^2$ | 3.91 |
| 30889 | 345 | 30887 | 350 | $45_0^2T_{x_0}^1$ | 2.66 |
| **30936** | **392** | **30939** | **389** | $\mathbf{45_0^4}$ | **1.86** |
| **30965** | **421** | **30969** | **419** | $\mathbf{44_0^145_0^1}$ | **2.23** |
| **30985** | **441** | **30982** | **432** | $\mathbf{43_0^145_0^1}$ | - |

To explore the extent of the above three processes in the electronically excited PBI-$H_2O$ system, the hole-burning (HB) spectrum of PBI-$H_2O$ and the R2PI spectrum of the PBI-$D_2O$ complex were recorded, as shown in Figure 1. In the HB spectra, the first scanning laser depletes the population of the vibrationless $S_0$ state at each Franck-Condon active $S_0 \rightarrow S_1$ transition, irrespective of the lifetime of the final state. The HB spectra recorded by monitoring the depletion of the R2PI signal at band origin can represent all the Franck-Condon active vibrational modes of $S_0 \rightarrow S_1$ transitions.

In the HB spectrum of PBI-$H_2O$, as shown in Figure 1 (trace c), the bands associated with the $S_0 \rightarrow S_1$ transition are observed till $0_0^0 + 1120$ $cm^{-1}$, confirming Franck-Condon activity on both the intra and intermolecular vibrational bands in the $S_1$ state. The intensity pattern of the intramolecular modes in the HB spectrum of PBI-$H_2O$ was found to be similar to that in the R2PI spectra of PBI. The above Franck-Condon activity in the PBI-$H_2O$ complex can be ruled out as a reason for the disappearance of the R2PI signal.

The intensities of the intermolecular modes in the R2PI spectrum of PBI-$H_2O$ near the 200-400 $cm^{-1}$ region are

significantly lower compared to the corresponding peaks in the HB spectrum. As mentioned earlier, the intermolecular vibrational modes are the internal translational motion of water molecules towards the $N_P$ ($\nu_{Ty}$) and $N_I$-H ($\nu_{Tx}$) groups. Therefore, quantum tunnelling of a proton/hydrogen is feasible, which can decrease the peak intensity of the intermolecular modes in R2PI spectra. The scope of tunnelling is further verified using the kinetic isotope effect in the PBI-$D_2O$ system.

**Kinetic Isotope Effect:** The R2PI spectrum of the PBI-$D_2O$ complex is shown in Figure 1(d). The isotopic H/D substitution generally makes a negligible structural change in the structures of a complex in the ground and excited electronic states and the properties of electronic transitions. The above is evident from the marginal blue shift of 6 $cm^{-1}$ of the $0_0^0$ band with respect to that of the PBI-$H_2O$ complex (Table 2), and it gives excellent agreement with the calculated value of 5 $cm^{-1}$. The rate of quantum tunnelling can be significantly decreased due to the high mass of the D/$D^+$, and the effect can be accounted for by the enhanced intensity of the intermolecular bands in the spectrum. Secondly, H/D substitution can significantly reduce the zero-point vibrational energy of an electronic state of molecules and hence, the activation energy of a reaction can be elevated. Previous studies of the 7-hydroxyquinoline-$(CH_3OH)_2$ system demonstrated an 8-16 kJ $mol^{-1}$ increase in the activation energy of NH···O and OH···O double proton transfer barrier.[37]

The R2PI spectrum of PBI-$D_2O$ shows visible transitions up to $0_0^0 + 1030$ $cm^{-1}$. Thus, the excited state energy barrier is expected to be as high as 1030 $cm^{-1}$, which is much higher than that observed in the PBI-$H_2O$ complex. The intensities of the transitions in PBI-$D_2O$ are found to be similar to that observed in the HB spectrum of PBI-$H_2O$. The intensities of the intramolecular vibrational modes before the cut-off band of $0_0^0 + 421$ $cm^{-1}$ is found to be similar to that in the $H_2O$ complex. However, the intensities of intermolecular modes in PBI-$D_2O$ above 200 $cm^{-1}$ are significantly enhanced. The above enhancement of peak intensity can be directly linked to the slower/negligible quantum tunnelling of D/$D^+$ in the PBI-$D_2O$ complex. This implies that the lifetimes of the excited vibrational states have increased significantly upon isotopic substitution because of the low quantum tunnelling rate.

The above observations clearly established the possibility of quantum mechanical tunnelling in the PBI-$H_2O$ complex, mainly for the transitions associated with the intermolecular modes. The isotopic substitution has not only decreased the rate of quantum tunnelling but has also elevated the energy barrier associated with the excited state processes.

To understand the rate of quantum tunnelling in different vibrational modes in the PBI-$H_2O$ complex, we have calculated the ratio of the peak intensities of the R2PI bands of PBI-$D_2O$ with that of PBI-$H_2O$ as $\frac{I_D}{I_H} = \frac{I_{PBI-D_2O}}{I_{PBI-H_2O}}$ and the ratios are given in Table 2. SI Figure S2 shows the comparison of the baseline-corrected normalised spectra used for the above calculation. The intramolecular bands at 274 and 392 $cm^{-1}$ have shown $\frac{I_D}{I_H}$ intensity ratios of 1.40 and 1.86, respectively. The intermolecular bands in the same region, positioned at 263 ($\nu_{45}$+$\nu_{Ty}$), 303 ($2\nu_{Tx}$) and 345 $cm^{-1}$ ($\nu_{45}$+$2\nu_{Tx}$), have shown the $\frac{I_D}{I_H}$ values of 3.91, 3.91 and 2.66, respectively. Therefore, the intermolecular bands in PBI-$H_2O$ show an enhanced quantum tunnelling effect, which is suppressed upon D-substitution because of the kinetic isotope effect. The above confirms the presence of strong quantum mechanical tunnelling in the PBI-$H_2O$ system, which is induced by the intermolecular vibrational motion mainly. The only intramolecular band $\nu_{44}$+$\nu_{45}$ at 421 $cm^{-1}$ has shown a high $\frac{I_D}{I_H}$ ratio of 2.23. In addition to the above, the absence of any intramolecular modes above $0_0^0 + 421$ $cm^{-1}$ region must be due to the proximity of an excited state energy barrier rather than the effect of only the quantum tunnelling.

**Table 3.** The calculated excited state energy barriers (kJ $mol^{-1}$) in PBI-$H_2O$, PBI-$D_2O$ and PBI-$NH_3$ complexes are given. The values in parentheses represent the ZPE corrected values.

| Energy | PBI-$H_2O$ | PBI-$D_2O$ | PBI-$NH_3$ |
|---|---|---|---|
| $\Delta E^{\#}$ (espt) | 10.5 *(6.8)* | 10.5 *(10.3)* | 19.6 |
| $\Delta E^{\#}$ (esht) | 15.9 *(17.2)* | - | 16.5 |
| $\Delta E^{\#}(S_1)$ (expt) | **5.2±0.1** | **>12.3** | **>10.4** |

Overall, the hole-burning spectrum (Figure 1c) confirms the presence of Franck-Condon activity in the complex beyond 421 $cm^{-1}$. Secondly, the reappearance of the Franck-Condon activity in PBI-$D_2O$ above $0_0^0 + 421$ $cm^{-1}$ confirms the elevation of the energy barrier upon isotopic substitution. The cut-off band at 421 $cm^{-1}$ in the PBI-$H_2O$ complex, assigned as the $\nu_{45} + \nu_{43}$ mode, is also observed at 419, 419 and 422 $cm^{-1}$ in bare PBI, PBI-$D_2O$ and PBI-$NH_3$ spectra, respectively. Therefore, the $0_0^0 + 421$ $cm^{-1}$ band can be picked as the lower limit of the excited state energy barrier in the PBI-$H_2O$ system. The adjacent intramolecular mode detected in the HB spectrum of PBI-$H_2O$ is a combination of $\nu_{43}$+$\nu_{45}$ at 441 $cm^{-1}$. The same band is also observed at the same position in the spectra of PBI, PBI-$D_2O$ and PBI-$NH_3$ complexes.

Therefore, the ESPT energy barrier in PBI-$H_2O$ can be bracketed as 431±10 $cm^{-1}$ (5.2±0.1 kJ$mol^{-1}$, Table 3). In the case of the PBI-$D_2O$ complex, the last peak in the R2PI spectrum detected with confidence is positioned at $1030$ $cm^{-1}$ (12.3 kJ $mol^{-1}$) above the origin band, which can be considered as the lower limit of the excited state energy barrier. The ZPE-corrected proton transfer energy barrier in PBI-$D_2O$ in the $S_1$ state (10.3 kJ$mol^{-1}$) was found to be close to the experimental data.

Additionally, the intensity pattern of the PBI-$D_2O$ R2PI spectrum was different than the hole-burning spectrum of the PBI-$H_2O$ complex in the higher energy region due to possible quantum tunnelling of $D^+$ at the higher energy region. As discussed above, the tunnelling rate of $D^+$ was significantly lower than that of $H^+$; however, the rate constant value cannot be negligible. Secondly, at the higher energy region, the rate of tunnelling increases significantly. The above can be the reason

for the less intense R2PI peaks above 600 $cm^{-1}$ in the PBI-$D_2O$ system.

**Excited state processes in PBI-$NH_3$:** Based on the PBI-$NH_3$ structure in the $S_1$ state, one can expect lower tunnelling rate proton/hydrogen of solvent to $N_P$ and a higher energy barrier due to the wider potential along the $N_P\cdots H_b$ distance. The R2PI spectrum of the PBI-$NH_3$ complex in Figure 1e is drastically different than that of the water complex. It shows the $S_0 \rightarrow S_1$ transition spanned over $0_0^0 + 868$ $cm^{-1}$ with highly intense ion signals above $0_0^0$ +421 $cm^{-1}$. The above is in full accordance with the above expectation of low tunnelling and a higher energy barrier.

The Franck-Condon simulated spectrum using the most stable structure, as shown in SI Figure S3, has shown good agreement with the recorded spectrum in terms of peak positions and intensities. The HB spectrum has shown nearly similar depletion patterns as that of the R2PI spectrum for each band till 733 $cm^{-1}$. Importantly, the intensity of the R2PI peaks associated with the intermolecular modes is found to be as strong as the adjacent intramolecular ones. The above reveals negligible quantum tunnelling in the energy region up to 733 $cm^{-1}$ above the origin band. The above confirms (a) the higher energy barriers for the excited state processes in the PBI-$NH_3$ complex and (b) the quantum mechanical tunnelling is significantly suppressed in the system. Based on the last observed band in the spectrum, we can conclude that, in the PBI-$NH_3$ system, a minimum of 868 $cm^{-1}$ (10.4 kJ $mol^{-1}$) is required to access the excited state processes. The ESPT energy barrier in PBI-$H_2O$ was only $431\pm10$ $cm^{-1}$, which increased significantly (>868 $cm^{-1}$) in the PBI-$NH_3$ complex. To further investigate the underlying explanation of such drastic changes in the excited state energy barriers upon solvent substitution, we have further analysed the above processes computationally.

**ESPT vs ESHT processes:** In the PBI-$H_2O$ complex, the quantum tunnelling is profound mainly on the intermolecular modes, in which the solvent has shown internal translation motion towards $N_P$ and $N_IH$ groups.

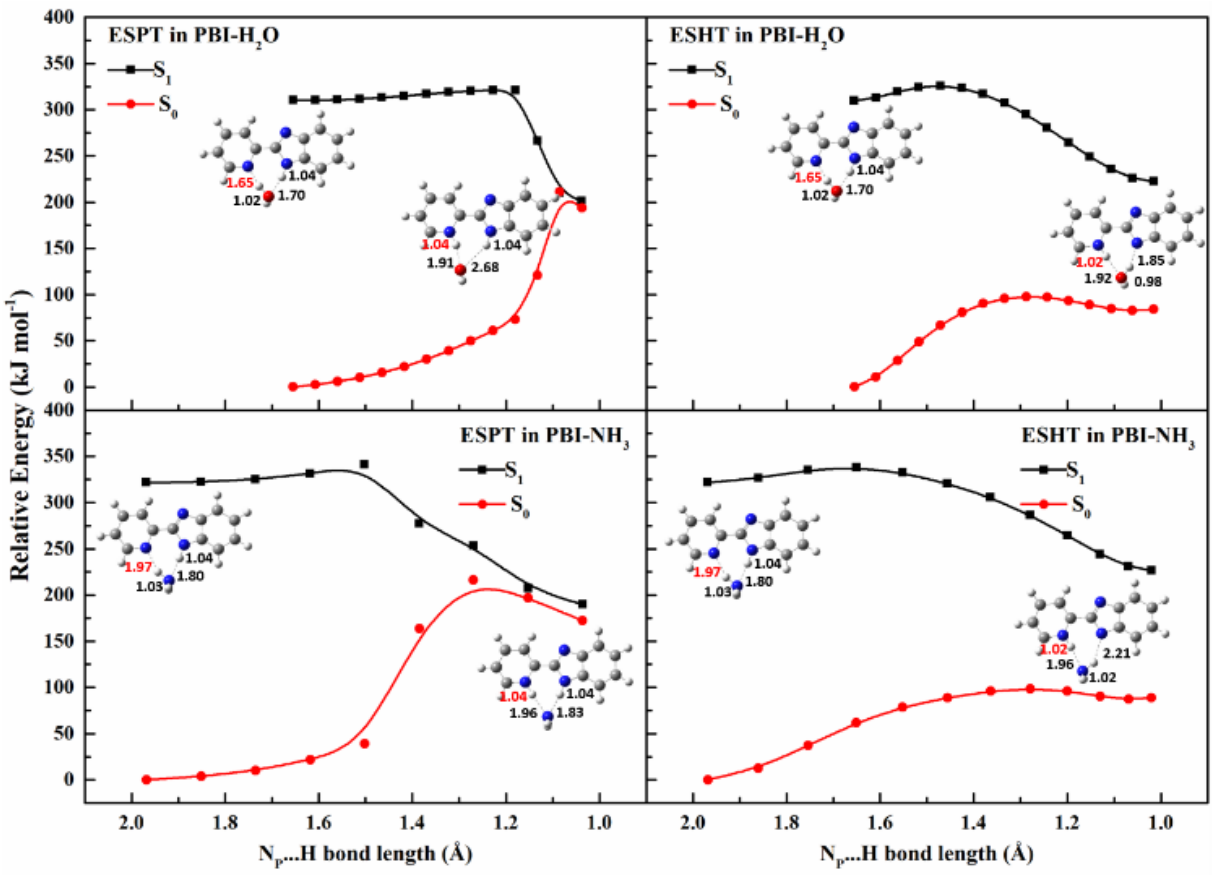


**Figure 4**. Potential energy profile calculated at DFT-D4/B3-LYP (def2-TZVPP) for the electronic ground state ($S_0$) and the locally excited ($S_1$) state of PBI–$H_2O$ (bottom) and PBI-$NH_3$ (top) as a function of the $N_P\cdots H$ bond length along the proton-transfer (left) and hydrogen transfer (right) coordinate for the reaction path optimisation (red star). The optimised geometry of initial (normal form) and the final structure (tautomer or protonated product) along the path are also shown. Note that the protonated product along the ESPT channel are not the real minima as it results in one imaginary frequency along the proton transfer coordinate ($N_P\cdots HO$).

In order to investigate the possibility of concerted double hydrogen atom transfer (ESHT) or proton transfer (ESPT) from solvent to PBI, potential energy surfaces were obtained along the hydrogen and proton transfer coordinates N/OH···$N_P$ and $N_IH$···(O/N) in PBI-S complexes and the 1D-PESes are given in Figure 4.

To further verify the nature of the transfer reactions, we have calculated the excited state NBO charge analysis after the gradient optimization step. Here the charge is calculated at the OH and $NH_2$ units for $H_2O$ and $NH_3$ complexes, respectively, along the reaction pathway (as shown in SI Figure S5). Here, the relative NBO charge of $OH/NH_2$ moiety in the respective complex in the $S_1$ state was calculated as $\Delta q=q_i-q_r$. Where $q_i$ is the total NBO charge on $OH/NH_2$ in the structures along the path, and $q_r$ is the NBO charge on $OH/NH_2$ in the first structure in the $S_1$ state. A proton transfer must be accompanied by a negative charge accumulation at the $OH/NH_2$ moiety. As shown in the figure SI Figure S5, the ESPT reaction pathway shows drastic negative charge accumulation on the solvent unit in both PBI-$H_2O$ and PBI-$NH_3$ complexes. In the case of the ESHT reaction pathway, the solvent unit becomes weakly positive, most likely due to the electrostatic hydrogen bonding interactions. Therefore, the second pathway cannot be described as a double proton transfer reaction.

The ESHT product is the tautomer with the $N_PH$ group, which is found to be more stable by ~80 kJ $mol^{-1}$ than that of the normal form (with $N_IH$ group). The reaction proceeds via the simultaneous hydrogen atom transfers from $N_IH$ to the solvent molecule and from the solvent to the $N_P$ group. In the case of the proton transfer process, the PES is generated by transferring a proton to the $N_P$ while keeping the $N_I$-H bond distance constant. A detailed analysis of the reaction was recently reported for the PBI-$H_2O$ system.[16] The ESPT and ESHT energy barriers (Table 3) in the PBI-$H_2O$ are 10.5 and 15.9 kJ $mol^{-1}$. The ZPE corrected values are found to be 6.8 and 10.3 kJ $mol^{-1}$, respectively. The above ESPT value shows a better agreement with the current experimental data of 5.2±0.1 $kJmol^{-1}$. In the system, the barrier was characterised as an intersection of ππ* and nπ* states. To further elaborate the role of ππ* and nπ* states on the ESPT mechanism, the potential energy surface for the electronic ground state ($S_0$) and the locally excited ππ* and nπ* states of the PBI–$H_2O$ are plotted as a function of the concerted stretching of the OH···$N_P$ ($N_P$ = pyridinyl N) distances along the ESPT pathway (SI Figure S4). In the figure, the intersection of the ππ* and nπ* states are clearly visible along the pathway. A subsequent barrierless internal conversion process was found to deactivate the molecule to the ground state. The above can drastically reduce the lifetime of the excited vibrational states above the barrier. The processes can be the reason for the drastic disappearance of the intramolecular bands in the PBI-$H_2O$ spectrum beyond the cut-off region.

In the case of the PBI-$NH_3$ system (Table 3 and Figure 4), the ESPT and ESHT energy barriers were calculated to be 19.6 and 16.5 kJ $mol^{-1}$. Therefore, the ESHT may have a marginally lower energy barrier than the competing ESPT processes. Optimising the transition state structures in the $S_1$ state of the PBI-$NH_3$ complex has failed after repeated attempts, and hence the ZPE corrected values were not possible at the current level of theory. The calculated energy barriers of ESPT and ESHT processes were found to be higher than the experimentally observed possible lower limit of 10.4 kJ $mol^{-1}$. The uncorrected ESPT energy barrier in PBI-$NH_3$ has shown a significantly higher value than that observed in the PBI-$H_2O$ complex. Note that, being a poor hydrogen bond donor, as evident from the structure of the PBI-$NH_3$ complex, the width of the proton transfer pathway along the NH···$N_P$ coordinate is significantly longer than that in the PBI-$H_2O$ complex. The above is the most likely reason for both the higher energy barrier and lower quantum tunnelling rate of the proton transfer process in the PBI-$NH_3$ complex.

## Conclusions

The R2PI spectra of $S_0 \rightarrow S_1$ transition of PBI, PBI-$H_2O$, PBI-$D_2O$, and PBI-$NH_3$ were recorded by monitoring the m/z of 195, 213, 215 and 212 in separate experiments. The hole-burning spectroscopy confirmed that each band system in a spectrum is originated from a single isomer present in the molecular beam. The geometry optimisation at B3LYP-D4/def2-TZVPP level of theory, in combination with experimental data, resulted in the most stable structures of PBI-$H_2O$ and PBI-$NH_3$ complexes with $N_IH$···O and OH···$N_P$ ($N_P$ = pyridinyl N) hydrogen bonds. The experimentally measured frequency of $\nu_{Ty}$, i.e., the internal translational motion of $H_2O$ along (HO)H···$N_P$ hydrogen bond was observed at 168 $cm^{-1}$. The corresponding bond in PBI-$NH_3$ was obtained at a much lower frequency at 115 $cm^{-1}$, confirming a feebly bound NH···$N_P$ hydrogen bond.

The R2PI spectrum of PBI-$H_2O$ shows a decrease in intensity of the intermolecular modes near the cut-off region, i.e., $0_0^0 + 421$ $cm^{-1}$, before being disappeared completely. In the HB spectrum of PBI-$H_2O$, the non-zero Franck-Condon factors for the $S_0 \rightarrow S_1$ transition are observed till $0_0^0 + 1120$ $cm^{-1}$. The ESPT energy barrier in the complex was thus bracketed at 5.2±0.1 kJ $mol^{-1}$ (431±10 $cm^{-1}$) in the $S_1$ state. The experimental value was excellently complemented by the calculated ESPT energy barrier of 6.8 kJ $mol^{-1}$.

The intensities of the intermolecular modes, coupled with the intramolecular vibrations near the 300-421$cm^{-1}$ region, were lower compared to the corresponding peaks in the HB spectrum. The decreasing intensities of the bands were due to the enhanced quantum tunnelling of a proton from solvent to $N_P$ of PBI near the ESPT barrier. The R2PI spectrum PBI-$D_2O$ displayed intense peak intensities of the transitions related to the intermolecular modes in the $S_1$ state, confirming the quantum tunnelling effect triggered by such vibrational modes. The isotopic substitution had shown a significant slowdown of the quantum tunnelling rate due to the heavy mass of deuterium. The extent of kinetic isotopic substitution, calculated from the R2PI peak intensities in PBI-$D_2O$ and PBI-$H_2O$ systems, confirmed the above. The H/D isotopic substitution elevated the excited state energy barrier drastically by lowering the zero-point energy of the $S_1$ state. The ESHT energy barrier in PBI-$H_2O$ was calculated to be significantly

higher (15.9 (17.2) kJ mol$^{-1}$) than that of ESPT. In the system, the barrier was characterised as an intersection of ππ* and nπ* states. A subsequent barrierless internal conversion process was found to deactivate the molecule to the ground state.

The R2PI spectrum of PBI-$NH_3$ displayed a negligible tunnelling rate for the bands till $0_0^0 + 700\,cm^{-1}$, confirmed using hole-burning spectroscopy. Additionally, the ESPT energy barrier (>10.4 kJ mol$^{-1}$) in PBI-$NH_3$ was significantly higher than that observed in the PBI-$H_2O$ complex. Here, being a poor hydrogen bond donor, the width of the proton transfer pathway was much longer than that in the PBI-$H_2O$ complex, which resulted in the higher energy barrier and lower quantum tunnelling rate of the excited state proton transfer energy barrier in the PBI-$NH_3$ complex. The current experimental schemes can be used to determine various fundamental parameters of excited state processes, such as energy barriers, relative quantum tunnelling rates, and the kinetic isotope effect. Secondly, the variation observed for both energy barrier and quantum tunnelling rate by substituting $NH_3$ in place of $H_2O$ can be directly correlated to the drastically different photo-chemical and photo-physical reactions of biomolecules under various microenvironments.

## Author Contributions

All authors have given approval for the final version of the manuscript.
‡These authors contributed equally.
SK and JR performed the experiments with the help of SB, MS and BK. SK and JR did the data analysis and computational calculations. SK, JR and SM wrote the manuscript.

## Conflicts of interest

There are no conflicts to declare.

## Acknowledgements

This work has been supported by the Department of Chemistry, IIT Hyderabad and MHRD, the Government of India. SK thanks MHRD, India, for the research fellowship. JR and BK thank UGC for the research fellowship. SB and MS thank MoE for the research fellowship. SM expresses sincere gratitude towards Prof. Samuel Leutwyler, the University of Bern, for his generous instrumentation aid to IITH for the experimental set-up. SM thanks SERB, DST government of India (Grant no. CRG/2019/003335) for funding.

## Supporting Information

Supporting Information contains FC-simulated spectra, comparison between normalized R2PI spectra of PBI-$H_2O$ and PBI-$D_2O$, DFT-D4 (B3-LYP/def2-TZVPP) computed potential energy surfaces in PBI-$H_2O$ along ESPT showing intersection of the ππ* and nπ* states, NBO charge analysis, spectral assignments for PBI-$NH_3$ and Coordinates of the optimized structures of PBI monomer, PBI–$H_2O$ and PBI-$NH_3$ complex.

## Notes and references

1 J. M. L. Pecourt, J. Peon and B. Kohler, DNA excited-state dynamics: Ultrafast internal conversion and vibrational cooling in a series of nucleosides, *J. Am. Chem. Soc.*, 2001, **123**, 10370–10378.
2 W. M. Kwok, C. Ma and D. L. Phillips, Femtosecond time- and wavelength-resolved fluorescence and absorption spectroscopic study of the excited states of adenosine and an adenine oligomer, *J. Am. Chem. Soc.*, 2006, **128**, 11894–11905.
3 W. J. Schreier, P. Gilch and W. Zinth, Early events of DNA photodamage, *Annu. Rev. Phys. Chem.*, 2015, **66**, 497–519.
4 Y. Zhang, K. De La Harpe, A. A. Beckstead, L. Martínez-Fernández, R. Improta and B. Kohler, Excited-State Dynamics of DNA Duplexes with Different H-Bonding Motifs, *J. Phys. Chem. Lett.*, 2016, **7**, 950–954.
5 X. Wang, Y. Yu, Z. Zhou, Y. Liu, Y. Yang, J. Xu and J. Chen, Ultrafast Intersystem Crossing in Epigenetic DNA Nucleoside 2′-Deoxy-5-formylcytidine, *J. Phys. Chem. B*, 2019, **123**, 5782–5790.
6 X. Wang, Z. Zhou, Y. Tang, J. Chen, D. Zhong and J. Xu, Excited State Decay Pathways of 2′-Deoxy-5-methylcytidine and Deoxycytidine Revisited in Solution: A Comprehensive Kinetic Study by Femtosecond Transient Absorption, *J. Phys. Chem. B*, 2018, **122**, 7027–7037.
7 C. E. Crespo-herna, B. Cohen, P. M. Hare and B. Kohler, Ultrafast excited-state dynamics in nucleic acids Chem. Rev. 2004, 104, 1977−2019.pdf, *Chem. Rev.*, 2019, **104**, 1977–2019.
8 T. Schultz, E. Samoylova, W. Radloff, I. V. Hertel, A. L. Sobolewski and W. Domcke, Efficient deactivation of a model base pair via excited-state hydrogen transfer, *Science.* 2004, **306**, 1765–1768.
9 A. Douhal, S. K. Kim and A. H. Zewail, Femtosecond molecular dynamics of tautomerization in model base pairs, *Nature*, 1995, **378**, 260–263.
10 C. Jouvet, M. Miyazaki and M. Fujii, Revealing the role of excited state proton transfer (ESPT) in excited state hydrogen transfer (ESHT): systematic study in phenol-(NH3)nclusters, *Chem. Sci.*, 2021, **12**, 3836–3856.
11 R. Knochenmuss, O. Cheshnovsky and S. Leutwyler, Proton transfer reactions in neutral gas-phase clusters: 1-Naphthol with H2O, D2O, CH3OH, NH3 and piperidine, *Chem. Phys. Lett.*, 1988, **144**, 317–323.
12 E. Samoylova, V. R. Smith, H. H. Ritze, W. Radloff, M. Kabelac and T. Schultz, Ultrafast deactivation processes in aminopyridine clusters: Excitation energy dependence and isotope effects, *J. Am. Chem. Soc.*, 2006, **128**, 15652–15656.
13 C. Tanner, C. Manca and S. Leutwyler, Probing the Threshold to H Atom Transfer Along a Hydrogen-Bonded Ammonia Wire, *Science.* 2003, **302**, 1736–1739.
14 W. Domcke and A. L. Sobolewski, Unraveling the Molecular Mechanisms of Photoacidity, *Science.*, 2003, **302**, 1693–1694.
15 W. Sheng, M. Nairat, P. D. Pawlaczyk, E. Mroczka, B. Farris,

E. Pines, J. H. Geiger, B. Borhan and M. Dantus, Ultrafast Dynamics of a "Super" Photobase, *Angew. Chemie - Int. Ed.*, 2018, **57**, 14742–14746.

16 S. Khodia and S. Maity, A combined experimental and computational study on the deactivation of a photo-excited 2,2′-pyridylbenzimidazole-water complex via excited-state proton transfer, *Phys. Chem. Chem. Phys.*, 2022, **24**, 12043–12051.

17 R. Knochenmuss and I. Fischer, Excited-state proton transfer in naphthol/solvent clusters: The current state of affairs, *Int. J. Mass Spectrom.*, 2002, **220**, 343–357.

18 S. R. Brishty, M. J. Hossain, M. U. Khandaker, M. R. I. Faruque, H. Osman and S. M. A. Rahman, *Front. Pharmacol. 2021, **12**, 1–49.*

19 G. S. Yellol, J. G. Yellol, V. B. Kenche, X. M. Liu, K. J. Barnham, A. Donaire, C. Janiak and J. Ruiz, Synthesis of 2-pyridyl-benzimidazole iridium(III), ruthenium(II), and platinum(II) complexes. study of the activity as inhibitors of amyloid-β aggregation and neurotoxicity evaluation, *Inorg. Chem.*, 2015, **54**, 470–475.

20 H. Dong, X. Liu, H. Yang, J. Zhao and Y. Zheng, Harnessing Excited-State Proton Transfer Reaction for 2-(6′-Hydroxy-2′-pyridyl)benzimidazole via Solvents, *ACS Appl. Bio Mater.*, 2021, **4**, 1950–1957.

21 M. Vaquero, N. Busto, N. Fernández-Pampín, G. Espino and B. García, Appended Aromatic Moieties Determine the Cytotoxicity of Neutral Cyclometalated Platinum(II) Complexes Derived from 2-(2-Pyridyl)benzimidazole, *Inorg. Chem.*, 2020, **59**, 4961–4971.

22 A. M. Mansour and K. Radacki, Antimicrobial properties of half-sandwich Ir(III) cyclopentadienyl complexes with pyridylbenzimidazole ligands, *Dalt. Trans.*, 2020, **49**, 4491–4501.

23 K. E. Prosser, S. W. Chang, F. Saraci, P. H. Le and C. J. Walsby, Anticancer copper pyridine benzimidazole complexes: ROS generation, biomolecule interactions, and cytotoxicity, *J. Inorg. Biochem.*, 2017, **167**, 89–99.

24 L. Maiore, M. C. Aragoni, C. Deiana, M. A. Cinellu, F. Isaia, V. Lippolis, A. Pintus, M. Serratrice and M. Arca, Structure–Activity Relationships in Cytotoxic AuI/AuIII Complexes Derived from 2-(2′-Pyridyl)benzimidazole, *Inorg. Chem.*, 2014, **53**, 4068–4080.

25 W. Domcke, J. Ehrmaier and A. L. Sobolewski, Solar Energy Harvesting with Carbon Nitrides and N-Heterocyclic Frameworks: Do We Understand the Mechanism?, *ChemPhotoChem*, 2019, **3**, 10–23.

26 S. Khodia and S. Maity, A combined spectroscopic and computational investigation on dispersion-controlled docking of Ar atoms on 2-(2′-pyridyl)benzimidazole, *Phys. Chem. Chem. Phys.*, 2021, **23**, 17992–18000.

27 Saurabh Khodia, Ramesh Jarupula and Surajit Maity, Accurate measurement of sequential Ar desorption energies from the dispersion-dominated Ar 1–3 complexes of aromatic molecules, *Phys. Chem. Chem. Phys. 2023, 25, 2510–2516.*

28 F. Furche, R. Ahlrichs, C. Hättig, W. Klopper, M. Sierka and F. Weigend, No Title, *Turbomole. WIREs Comput. Mol. Sci.*, 2014, **4**, 91.

29 S. Grimme, Density Functional Theory with London Dispersion Corrections, *WIREs Comput. Mol. Sci.*, 2011, **1**, 211.

30 A. Francés-Monerris, H. Gattuso, D. Roca-Sanjuán, I. Tuñón, M. Marazzi, E. Dumont and A. Monari, Dynamics of the excited-state hydrogen transfer in a (dG)·(dC) homopolymer: Intrinsic photostability of DNA, *Chem. Sci.*, 2018, **9**, 7902–7911.

31 Z. Lin, A. W. Kohn and T. Van Voorhis, Toward Prediction of Nonradiative Decay Pathways in Organic Compounds II: Two Internal Conversion Channels in BODIPYs, *J. Phys. Chem. C*, 2020, **124**, 3925–3938.

32 Y. Hirao, K. Ihara, Y. Ishibashi, E. G. Tiu, T. Asahi and T. Kubo, Mechanism and Kinetics of Fluorescence Quenching of Fluorene-Endcapped Butatriene: A Microspectroscopic Study of the Discrete State Constructed in Microcrystals, *J. Phys. Chem. C*, 2022, **126**, 1196–1203.

33 P. Roy Chowdhury, S. Khodia and S. Maity, Solvent assisted excited-state deactivation pathways in isolated 2,7-diazaindole-S1-3 (S = Water and Ammonia) complexes, *Spectrochim. Acta Part A Mol. Biomol. Spectrosc.*, 2022, **278**, 121285.

34 I. Pugliesi and K. Müller-Dethlefs, The use of multidimensional Franck-Condon simulations to assess model chemistries: A case study on phenol, *J. Phys. Chem. A*, 2006, **110**, 4657–4667.

35 M. A. Trachsel, S. Blaser, L. Siffert, T. Wiedmer and S. Leutwyler, Excited-state vibrations, lifetimes, and nonradiative dynamics of jet-cooled 1-ethylcytosine, *J. Chem. Phys.*, , DOI:10.1063/1.5116911.

36 M. R. Haggmark, G. Gate, S. Boldissar, J. Berenbeim, A. L. Sobolewski and M. S. de Vries, Evidence for competing proton-transfer and hydrogen-transfer reactions in the S1 state of indigo, *Chem. Phys.*, 2018, **515**, 535–542.

37 Y. Mori, Reaction pathway and H/D kinetic isotope effects of the triple proton transfer in a 7-hydroxyquinoline-methanol complex in the ground state: A computational approach, *J. Phys. Org. Chem.*, 2018, **31**, 1–12.